sustainability

MDPI

Article

Mohr–Coulomb and Modified Hoek–Brown Strength Criteria of Layered Sandstone Considering the Unloading Effect and Anisotropy

Zhixiang Song, Junwen Zhang * and Shaokang Wu

School of Energy and Mining Engineering, China University of Mining and Technology (Beijing), Beijing 100083, China; szxcumtb@126.com (Z.S.); wsk13037896248@126.com (S.W.)
* Correspondence: zhangjw@cumtb.edu.cn; Tel.: +86-13681359725

Abstract: The Mohr–Coulomb (M-C) and Hoek–Brown (H-B) strength criteria are widely used in various engineering fields, such as mining engineering, tunnel engineering and so on. To investigate the M-C and H-B strength criteria considering the unloading effect and anisotropy, series of triaxial loading (unloading) tests on layered sandstone were conducted. The results revealed that the peak strength was significantly affected by the unloading effect. Moreover, the cohesion and internal friction angle had a significant nonlinear relationship with the bedding angle. Additionally, the M-C and modified H-B strength criteria were established considering the unloading effect and anisotropy. Then, according to the strength criteria established, the peak strength could be estimated theoretically. Furthermore, compared to the M-C strength criteria, the modified H-B strength criteria were more appropriate for accurately estimating the triaxial compressive strength of layered sandstones. The conclusions obtained could provide certain references for the stability control of deep excavation engineering.

Keywords: M-C strength criteria; modified H-B strength criteria; layered sandstone; unloading effect; anisotropy

Citation: Song, Z.; Zhang, J.; Wu, S. Mohr–Coulomb and Modified Hoek–Brown Strength Criteria of Layered Sandstone Considering the Unloading Effect and Anisotropy. *Sustainability* **2023**, *15*, 14418. https://doi.org/10.3390/su151914418

Academic Editors: Kaihui Li, Dongya Han, Yanlin Zhao and Yu Chen

Received: 6 September 2023
Revised: 25 September 2023
Accepted: 28 September 2023
Published: 1 October 2023

1. Introduction

The M-C and H-B strength criteria are widely used in various engineering fields, including mining engineering, slope engineering, tunnel engineering, geothermal engineering, nuclear waste and CO_2 storage engineering [1–5]. The reason is that the essence of rock strength criteria refers to a theoretical basis for judging whether the yield or failure of rocks occurs under complex external loads. Moreover, it can visually represent the relationship between the stress state and rock strength.

In addition, the M-C and H-B strength criteria are widely used in rock mechanics. To verify the applicability and accuracy of strength criteria, numerous scholars conducted abundant studies with different perspectives and obtained abundant achievements. From the perspectives of porosity, lithology, density, rock composition and initial structures of rocks, serial strength criteria have already been constructed. Moreover, their applicability and accuracy have been verified [6–13]. Especially, the simple empirical strength criteria based on the uniaxial compressive strength of eight types of rocks and confining stress based on triaxial strength parameters were proposed [12]. In addition, the rock parameter of (m_i) in the Hoek–Brown strength criteria, from the perspective of the basic physical properties and factors of marlstones, sandstones and limestones, was evaluated and modified [8]. From the energy evolution perspective, the energy evolution mechanism of sandstone was deeply revealed based on the effect of confining pressure [14]. Meanwhile, the corresponding energy–strength criteria were established. Additionally, the yield criterion and modified compounded mobilized planes model were also constructed from the perspective of strain energy [15]. Meanwhile, the corresponding strength–energy criteria under

different stress conditions were established. Additionally, numerous scholars obtained certain innovative conclusions according to the rock strength criteria established from multiple perspectives with the strain rate effect, the effect of intermediate principal stress (including the effect of Lord's angle), the thermal effect, the bedding effect and the effect of hydrostatic pressure [16–35]. Specifically, series of true triaxial mechanical tests of rocks were conducted [27]. Moreover, the corresponding peak strength of rocks was obtained, and the nonlinear unified strength criterion considering the effect of intermediate principal stress was constructed [27]. Similarly, the nonlinear triaxial and poly-axial strength criteria for isotropic intact rocks considering the effect of intermediate principal stress were also constructed, and the applicability and accuracy of the criteria were verified [20]. Correspondingly, through introducing the weighting factor of the intermediate principal stress, the three-dimensional yield criteria were also simplified and established, which could effectively simulate the true triaxial strength of rocks under different stress levels [17].

However, the unloading effect is not considered in the above studies. In addition, there is significant anisotropy in the deep strata itself (see Figure 1a). Furthermore, there exists the obvious evolution process of the stress state of roadway surrounding rocks before excavation, during excavating and after excavation (see Figure 1b). Therefore, the stress path TLUT considering the unloading effect was proposed [36,37]. Furthermore, it was expected to improve the accuracy of the applicability of the strength criteria.

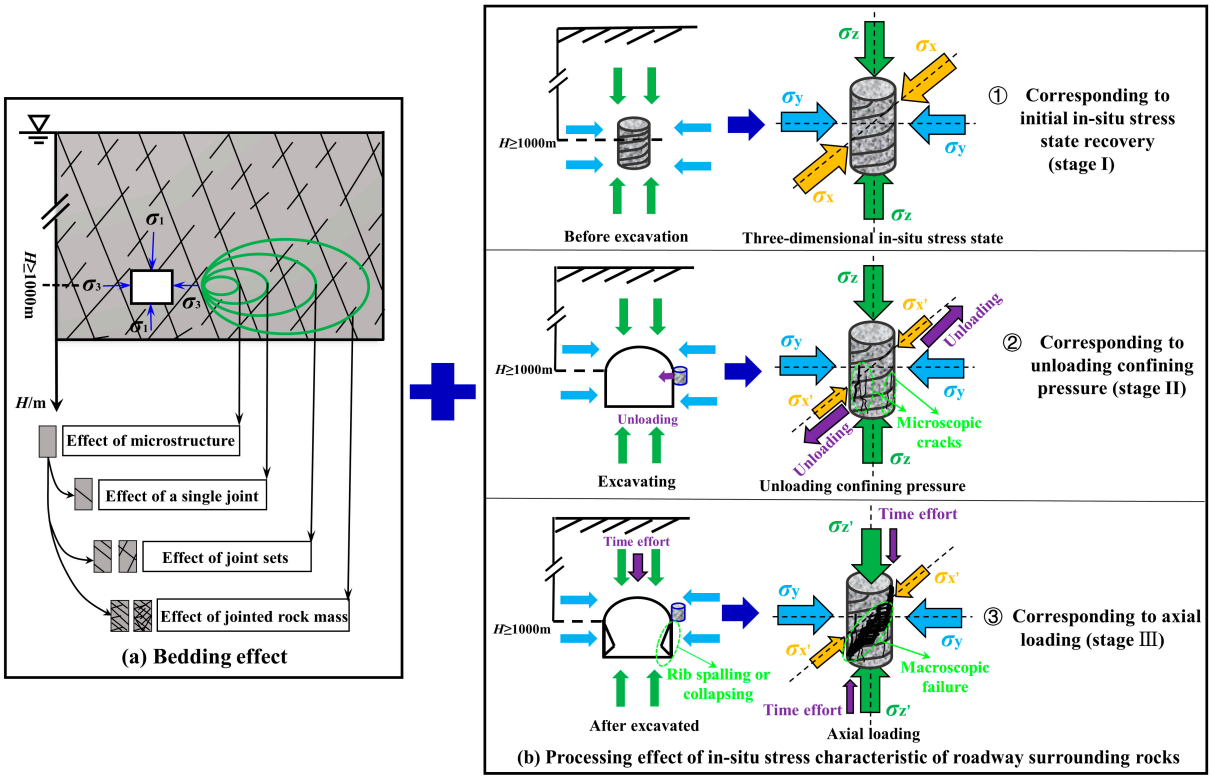

Figure 1. Engineering background [36,37]. Note: H, σ_1 and σ_3 represent the buried depth, axial stress and confining pressure, respectively; σ_x, σ_y, σ_z, $\sigma_{x'}$ and $\sigma_{z'}$ represent the minimum principal stress, the intermediate principal stress, the maximum principal stress, the minimum principal stress after unloading and the maximum principal stress after re-loading.

In this study, a series of triaxial loading tests considering the unloading effect and anisotropy was conducted, and the peak strength and deviator strength $(\sigma_1-\sigma_3)_{cf}$ could be measured. Based on analyzing the experimental data, it was indicated that the cohesion and internal friction angle were not constants and would change with increasing bedding angle. Furthermore, the specific expressions of the M-C and modified H-B strength criteria considering the unloading effect and anisotropy were established. The applicability of the

M-C and modified H-B strength criteria was verified by comparing the theoretical strengths with the actual experimental strengths.

2. Experimental System and Scheme

An MTS-815.02 electro-hydraulic servo rock mechanics test system was used in the tests, and the specific upper thresholds of basic parameters of the system are as follows:

a. The upper threshold of axial pressure is 1700 kN;
b. The upper threshold of confining pressure is 45 MPa;
c. The upper threshold of pore pressure is 45 MPa;
d. The upper threshold of osmotic water pressure difference is 2 MPa;
e. The upper threshold of osmotic gas pressure difference is 6 MPa;
f. The upper threshold of temperature is 200 °C;
g. The upper limit of specimen size for applicable tests is 100 mm in diameter and 200 mm in height.

Additionally, fully considering the excavation unloading effect of deep roadway surrounding rocks (see Figure 1), the stress path TLUT was designed and proposed, which broke through the awkwardness of the conventional triaxial loading stress path CTLT from zero loading to rock failure. The specific stress paths of uniaxial loading (UCT), conventional triaxial loading (CTLT) and triaxial loading and unloading (TLUT) are shown in Figure 2, and the detailed parameters settings of each stage of each sub-experiment are included. Among them, the stress state corresponding to the buried depth of 1010 m was the initial high in situ stress at the sampling site, and the specific detail of in situ stress measurement referred to [38].

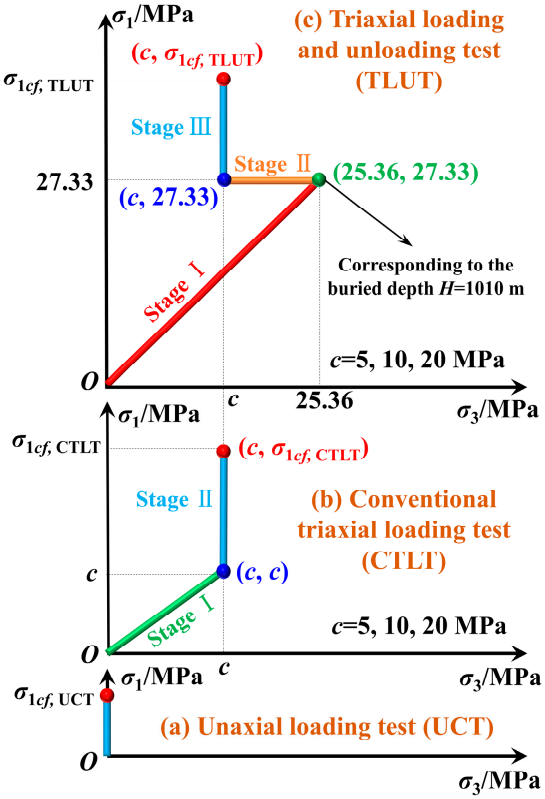

Detailed parameters

Stress paths	Stages division	Control models	Loading/Unloading rates
UCT	- -	Strain-controlled	Loading rate: 0.18 mm/min
CTLT	Stage Ⅰ	Stress-controlled	Loading rate: 5 MPa/min
	Stage Ⅱ	Strain-controlled	Loading rate: 0.18 mm/min
TLUT	Stage Ⅰ	Stress-controlled	Loading rate: 5 MPa/min
	Stage Ⅱ	Stress-controlled	Unloading rate: 5 MPa/min
	Stage Ⅲ	Strain-controlled	Loading rate: 0.18 mm/min

Figure 2. Stress paths and corresponding detailed parameters [38,39]. Note: c represents different pre-set confining pressures; $\sigma_{1cf,\mathrm{UCT}}$ represents uniaxial compressive strength of layered sandstones; $\sigma_{1cf,\mathrm{CTLT}}$ represents triaxial compressive strength of layered sandstones under CTLT; $\sigma_{1cf,\mathrm{TLUT}}$ represents triaxial compressive strength of layered sandstones under TLUT.

3. Results and Analysis

3.1. Strength Anisotropy

Referring to the literature [39], the peak strengths under UCT, CTLT and TLUT were obtained. Subsequently, the corresponding evolution characteristics of peak strength were drawn (see Figure 3).

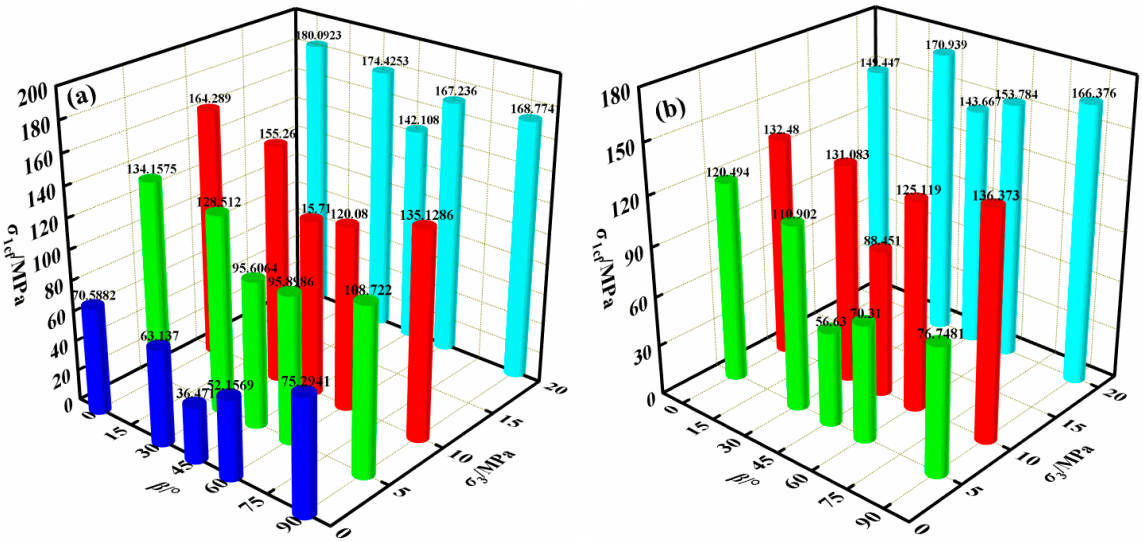

Figure 3. Peak strength evolution under different working conditions: (**a**) CTLT; (**b**) TLUT [38,39].

As shown in Figure 3, with increasing bedding angle, the peak strength first decreased and then increased. Among the angles, when the bedding angle was 45°, the peak strength was the smallest. Additionally, with increasing confining pressure, the peak strength also showed a continuous increasing nonlinear evolution trend.

Additionally, the peak strength under TLUT was significantly lower than that under CTLT. It indicated that the influences of the unloading effect on the peak strength were stronger than those of the effect of hydrostatic pressure. Corresponding to the whole life-cycle evolution process of deep roadway surrounding rocks, the unloading effect in excavation intensifies the released degree of a large amount of energy accumulated before excavation. Correspondingly, the dissipated energy is greatly improved during the unloading process. Meanwhile, its bearing capacity is further weakened by aggravating the damage degree of the roadway surrounding rocks. Therefore, it could be used, from the perspective of reducing the unloading effect in excavation, to start to improve the bearing capacity of roadway surrounding rocks. For example, before excavation, modern geophysical detection technology, geological big data, 5G communications, artificial intelligence and other technologies could be utilized to build a visual mine with high accuracy in real time [40–42]. Subsequently, series of structural regulation and measurement works could be conducted for the weak structures attached to the position of the roadway to be excavated by numerous technical means [43–45]. In this way, the bearing capacity of roadway surrounding rocks could be improved.

3.2. M-C and Modified H-B Strength Criteria

According to the above analysis, the unloading effect and bedding weak planes could both significantly affect the peak strength and bearing capacity of layered sandstones. Therefore, it was urgent to establish the M-C and H-B strength criteria considering the unloading effect and anisotropy. In this way, it could provide certain theoretical references for the stability control of deep excavation engineering.

3.2.1. Initial Principles of M-C Criteria

The two most important parameters in M-C strength criteria are the cohesion (c) and the internal friction angle (φ). As shown in Figure 4a, the relationship between the shear stress (τ) and the normal stress (σ_n) on arbitrary failure plane AB is as follows:

$$\tau = c + \sigma_n \tan \varphi \tag{1}$$

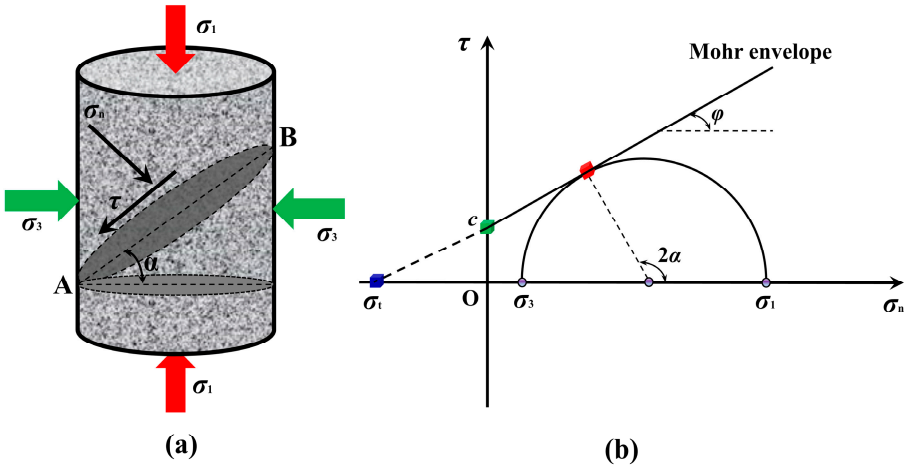

Figure 4. M-C strength criterion: (**a**) stress analysis; (**b**) strength envelope of shear and normal stresses [46,47].

Additionally, the shear stress (τ) and the normal stress (σ_n) can be obtained through stress transformation:

$$\begin{cases} \sigma_n = \frac{1}{2}(\sigma_1 + \sigma_3) + \frac{1}{2}(\sigma_1 - \sigma_3)\cos 2\alpha \\ \tau = \frac{1}{2}(\sigma_1 - \sigma_3)\sin 2\alpha \end{cases} \tag{2}$$

Coupling Equations (1) and (2) contributes to Equation (3):

$$\sigma_1 = \frac{2c + \sigma_3[\sin 2\alpha + \tan\varphi(1 - \cos 2\alpha)]}{\sin 2\alpha - \tan\varphi(1 + \cos 2\alpha)} \tag{3}$$

Furthermore, as shown in Figure 4b, the relationship between (α) and (φ) can be expressed as follows:

$$2\alpha = \frac{\pi}{2} + \varphi \tag{4}$$

Additionally, coupling Equations (3) and (4) contributes to Equation (5):

$$\sigma_1 = 2c \cdot \frac{\cos\varphi}{1 - \sin\varphi} + \frac{1 + \sin\varphi}{1 - \sin\varphi} \cdot \sigma_3 \tag{5}$$

According to Equation (5), the intercept (E) and the slope (F) can be obtained.

$$\begin{cases} E = \frac{2c \cdot \cos\varphi}{1 - \sin\varphi} \\ F = \frac{1 + \sin\varphi}{1 - \sin\varphi} \end{cases} \tag{6}$$

Meanwhile, according to Equation (6), (c) and (φ) can be obtained as follows:

$$\begin{cases} c = \frac{E}{2\sqrt{F}} \\ \varphi = \arcsin\frac{F-1}{F+1} \end{cases} \tag{7}$$

where τ and σ_n are the shear stress and the normal stress demonstrated on arbitrary failure plane AB; σ_1, σ_3 and σ_t are the axial stress, the confining pressure and the uniaxial tensile strength of materials, respectively. α is the angle between the direction of maximum principal stress and the failure plane AB. (c) and (φ) are the cohesion and the internal friction angle of materials.

3.2.2. M-C Strength Criteria

To further quantify the anisotropy on the peak strength, a functional relationship between the peak strength and the bedding angle was established. As shown in Figure 5, the fitting function relationship between the peak strength and the bedding angle under identical confining pressure is as follows:

$$\sigma_{1cf} = a + b * \beta + c * \beta^2 + d * \beta^3 + e * \beta^4 \quad (8)$$

where a, b, c, d and e are the fitting coefficients (see Table 1), β is the bedding angle, σ_{1cf} is the peak strength.

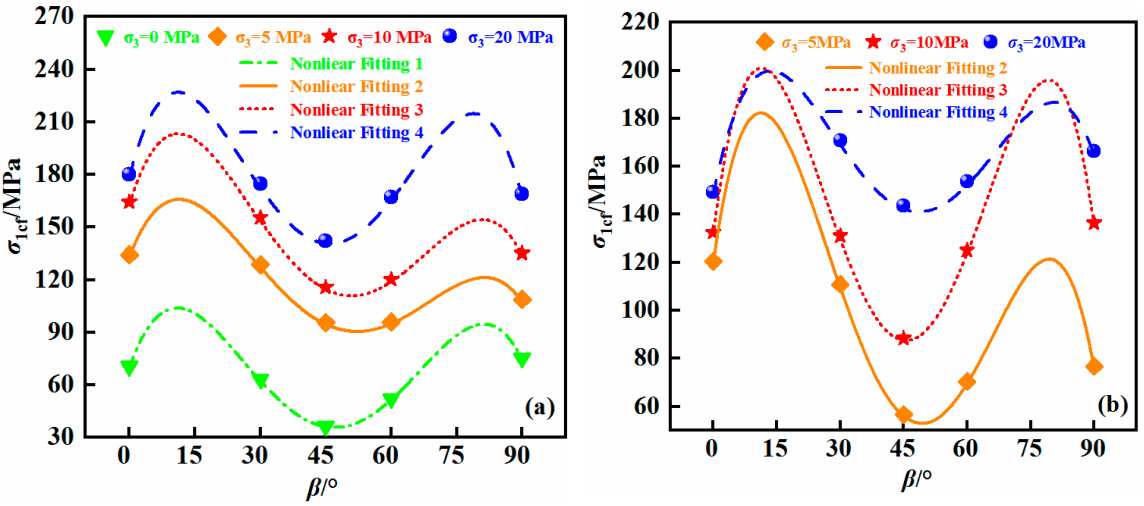

Figure 5. Fitting relationship between the peak strength and bedding angle under various confining pressures: (**a**) CTLT; (**b**) TLUT.

Table 1. Fitting functions between the peak strength and bedding angles under various confining pressures.

Stress Paths	σ_3/MPa	Fitting Functions	a	b	c	d	e	R^2
UCT	0	$\sigma_{1cf} = a + b * \beta + c * \beta^2 + d * \beta^3 + e * \beta^4$	69.882	7.008	−0.44	0.0078	-4.19×10^{-5}	0.99807
CTLT	5	$\sigma_{1cf} = a + b * \beta + c * \beta^2 + d * \beta^3 + e * \beta^4$	132.85	6.51	−0.39	0.0065	-3.37×10^{-5}	0.99504
	10	$\sigma_{1cf} = a + b * \beta + c * \beta^2 + d * \beta^3 + e * \beta^4$	162.65	8.18	−0.50	0.0085	-4.5×10^{-5}	0.99465
	20	$\sigma_{1cf} = a + b * \beta + c * \beta^2 + d * \beta^3 + e * \beta^4$	178.29	9.90	−0.62	0.011	-6.14×10^{-5}	0.98355
TLUT	5	$\sigma_{1cf} = a + b * \beta + c * \beta^2 + d * \beta^3 + e * \beta^4$	119.3	12.66	−0.77	0.01	-7.2×10^{-5}	0.99864
	10	$\sigma_{1cf} = a + b * \beta + c * \beta^2 + d * \beta^3 + e * \beta^4$	131.2	13.95	−0.85	0.02	-8.4×10^{-5}	0.99499
	20	$\sigma_{1cf} = a + b * \beta + c * \beta^2 + d * \beta^3 + e * \beta^4$	147.95	8.88	−0.47	0.008	-4.18×10^{-5}	0.97657

According to Table 1, the fitting coefficients all exceeded 0.9750, which indicated that there was a strong nonlinear relationship between the peak strength and bedding angles under identical confining pressure. Furthermore, compared with CTLT, the fitting curves of peak strength with TLUT fluctuated more significantly, which also indicated that the unloading effect significantly affected the accuracy of rock strength criterion.

The fitting relationship between the peak strength and the confining pressure under five different bedding angles is shown in Figure 6, and the corresponding details of fitting relationships can be seen in Table 2.

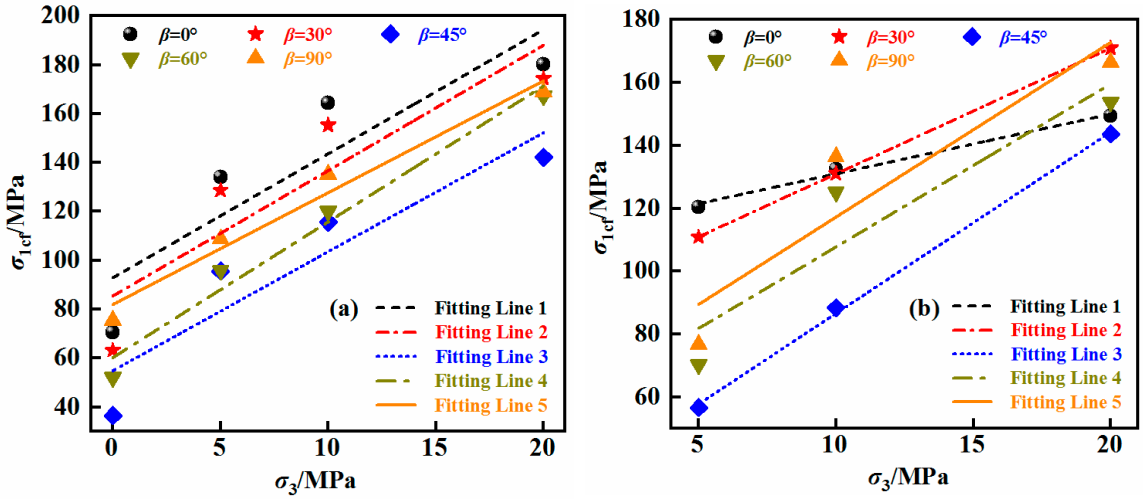

Figure 6. Fitting relationship between the peak strength and confining pressure under various bedding angles: (**a**) CTLT; (**b**) TLUT.

Table 2. Fitting functions between the peak strength and confining pressures under various bedding angles: CTLT and TLUT.

Stress Paths	*β*/°	Fitting Functions	*a*	*b*	R^2	*C*/MPa	*φ*/°
CTLT	0	$\sigma_{1cf} = a + b * \sigma_3$	92.85527	5.07731	0.80331	20.60438	42.1371
	30	$\sigma_{1cf} = a + b * \sigma_3$	85.45472	5.12911	0.81234	18.86623	42.3524
	45	$\sigma_{1cf} = a + b * \sigma_3$	54.84519	4.87182	0.85823	12.42404	41.2534
	60	$\sigma_{1cf} = a + b * \sigma_3$	60.22258	5.55663	0.97647	12.77390	44.0244
	90	$\sigma_{1cf} = a + b * \sigma_3$	81.93618	4.5764	0.97106	19.15066	39.8923
TLUT	0	$\sigma_{1cf} = a + b * \sigma_3$	112.0105	1.89684	0.99172	40.66431	18.0347
	30	$\sigma_{1cf} = a + b * \sigma_3$	90.974	4.0006	0.99999	22.74179	36.8733
	45	$\sigma_{1cf} = a + b * \sigma_3$	29.0247	5.76219	0.99869	6.04566	44.7680
	60	$\sigma_{1cf} = a + b * \sigma_3$	55.9759	5.17955	0.86989	12.29773	42.5592
	90	$\sigma_{1cf} = a + b * \sigma_3$	61.7466	5.55021	0.86333	13.10474	44.0006

As shown in Table 2 and Figure 6, compared with CTLT, the variation degree of slope and intercept of fitting lines of peak strength with TLUT was more significant. It still indicated that the unloading effect could significantly affect the evolution characteristics between the peak strength and the confining pressure. In addition, with increasing bedding angle, the slope of the fitting lines under CTLT showed an evolution trend that decreased first, then increased and finally decreased, but the variation degree was relatively slow. Meanwhile, the intercept of the fitting lines under CTLT showed a V-shaped evolution trend that decreased first and then increased, and the variation degree was more severe. However, with increasing bedding angle, the slope of the fitting lines under TLUT showed an increasing evolution trend, and the variation degree was relatively slow. Meanwhile, the intercept of the fitting lines under TLUT showed a V-shaped evolution trend that decreased first and then increased, and the variation degree was more significant. The above evolution characteristics indicated that the intercepts of the fitting lines under CTLT and TLUT were more sensitive to the anisotropy.

The Mohr circles and strength envelopes under CTLT and TLUT with five bedding angles are shown in Figures 7 and 8, respectively. When the bedding angle was constant, there was a significant tangential relationship between the Mohr strength envelope and the Mohr stress circle. According to the M-C strength criterion, the variation of slope and

intercept of the Mohr strength envelope was determined by the internal friction angle and the cohesion. Additionally, the internal friction angle and the cohesion with five bedding angles under CTLT and TLUT could be calculated according to Equation (7), and the calculation results are shown in Table 2.

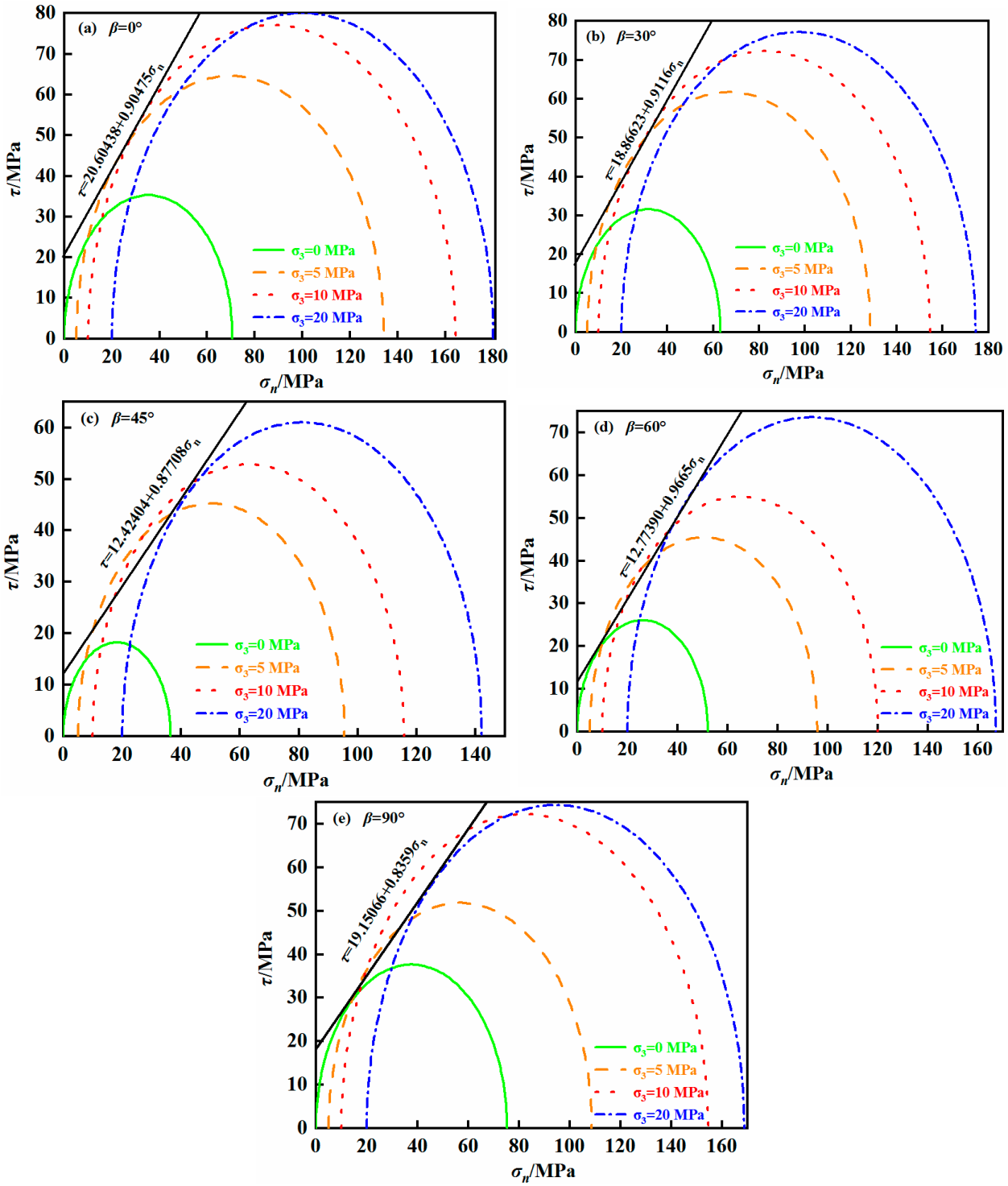

Figure 7. Mohr circles and strength envelopes under CTLT under different bedding angles: (**a**) $\beta = 0°$; (**b**) $\beta = 30°$; (**c**) $\beta = 45°$; (**d**) $\beta = 60°$; (**e**) $\beta = 90°$.

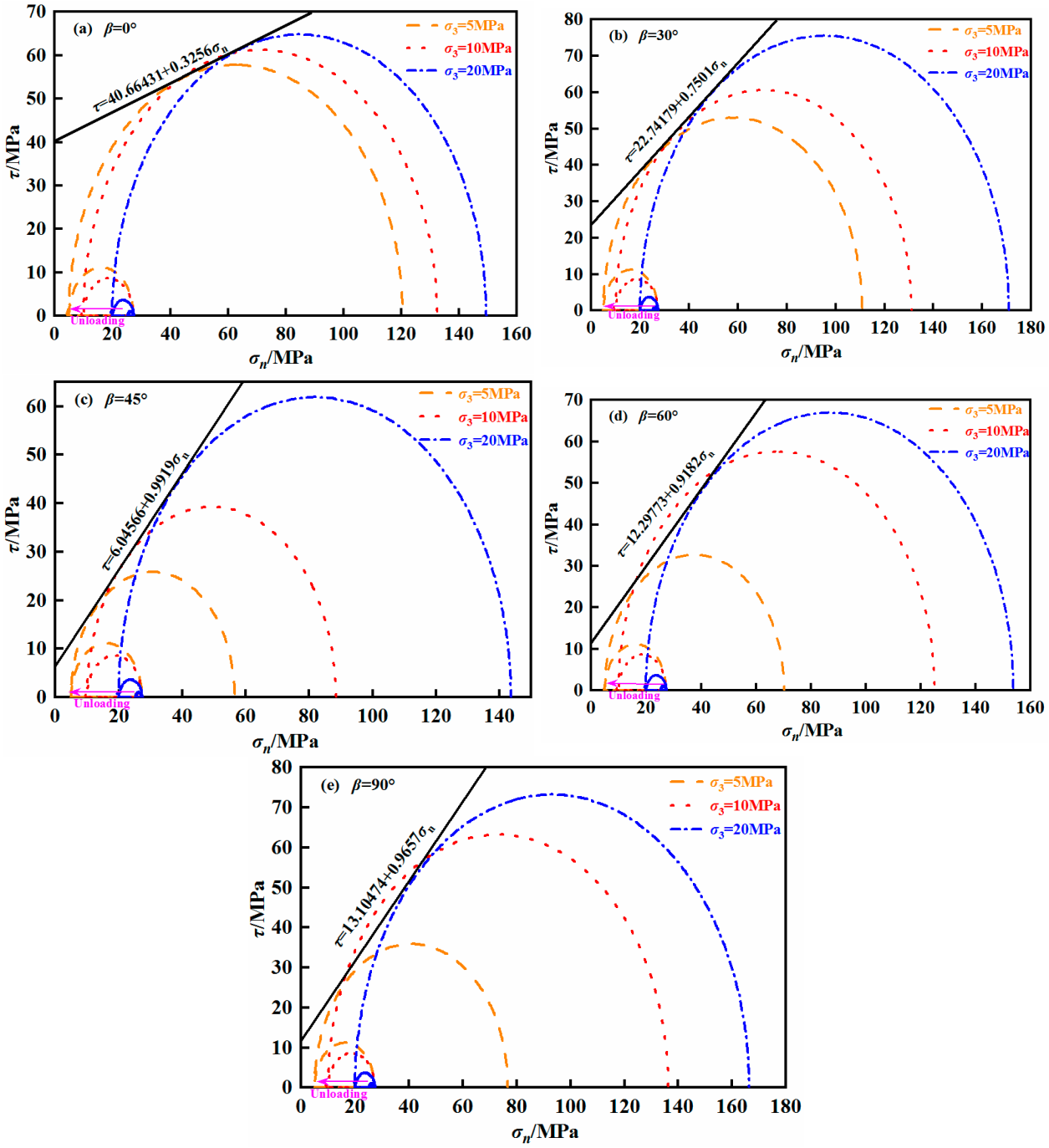

Figure 8. Mohr circles and strength envelopes under TLUT under different bedding angles: (**a**) $\beta = 0°$; (**b**) $\beta = 30°$; (**c**) $\beta = 45°$; (**d**) $\beta = 60°$; (**e**) $\beta = 90°$.

As shown in Table 2, with increasing bedding angle, the cohesion under CTLT presented a V-shaped evolution characteristic that sharply decreased first and then increased. Correspondingly, the internal friction angle fluctuated gently within $\varphi \in [39.8, 44]$. It indicated that the anisotropy on the cohesion was much greater than that of the internal friction angle. Namely, compared to the internal friction angle, the cohesion was more sensitive to the bedding effect. Similarly, with increasing bedding angle, the cohesion under TLUT also presented a V-shaped evolution characteristic that sharply decreased first and then increased. Correspondingly, the internal friction angle presented the evolution characteristic that sharply increased first and then remained basically constant. However, with increasing bedding angle, the variation degree of the cohesion under TLUT was sig-

nificantly higher than that of the internal friction angle. It also indicated that the cohesion was still more sensitive to the bedding effect compared to the internal friction angle. The above analysis showed that the unloading effect could significantly affect the evolution characteristic of the cohesion and the internal friction angle. Therefore, it was necessary to strengthen the study of strength criteria of rocks considering the unloading effect.

The variation of strength parameters with different bedding angles under CTLT and TLUT is shown in Figure 9. As shown in Figure 9, the cohesion and the internal friction angle under CTLT and TLUT showed a significant nonlinear polynomial function relationship with the bedding angle, and the specific expressions are as follows:

$$c_\beta = g + h * \beta + i * \beta^2 + j * \beta^3 \quad (9)$$

$$\varphi_\beta = p + q * \beta + r * \beta^2 + s * \beta^3 + t * \beta^4 \quad (10)$$

where g, h, i, j, p, q, r, s and t are all relevant fitting coefficients, and the specific values are shown in Tables 3 and 4. (c) and (φ) are the cohesion and the internal friction angle.

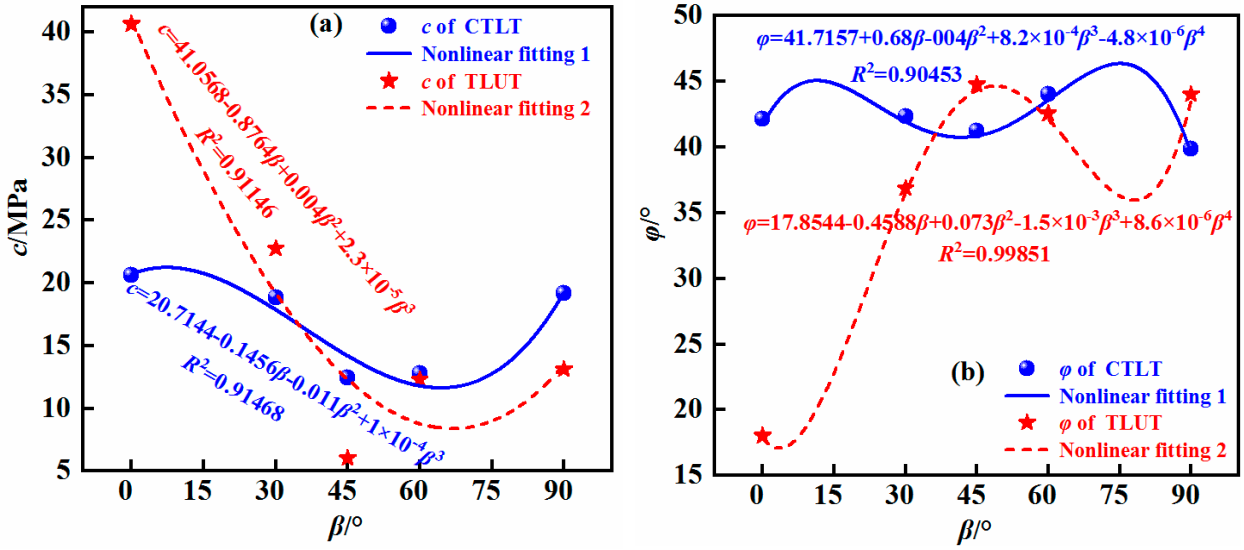

Figure 9. Variation of strength parameters with different bedding angles under CTLT and TLUT: (**a**) cohesion (c); (**b**) internal friction angle (φ).

Table 3. Fitting functions between (c) and β under CTLT and TLUT.

Stress Paths	Fitting Functions	g	h	i	j	R^2
CTLT	$c_\beta = g + h * \beta + i * \beta^2 + j * \beta^3$	20.714	−0.1456	−0.011	1×10^{-4}	0.91468
TLUT	$c_\beta = g + h * \beta + i * \beta^2 + j * \beta^3$	41.057	−0.8764	0.004	2.3×10^{-5}	0.91146

Table 4. Fitting functions between (φ) and β under CTLT and TLUT.

Stress Paths	Fitting Functions	p	q	r	s	t	R^2
CTLT	$\varphi_\beta = p + q * \beta + r * \beta^2 + s * \beta^3 + t * \beta^4$	41.7157	0.68	−0.004	8.2×10^{-4}	-4.8×10^{-6}	0.90453
TLUT	$\varphi_\beta = p + q * \beta + r * \beta^2 + s * \beta^3 + t * \beta^4$	17.8544	−0.4588	0.073	-1.5×10^{-3}	8.6×10^{-6}	0.99851

Coupling Equations (5), (9) and (10), the M-C strength criteria considering the bedding effect and the effect of confining pressure could be obtained as follows:

$$\sigma_{1cf\beta} = 2c_\beta \cdot \frac{\cos(\varphi_\beta)}{1 - \sin(\varphi_\beta)} + \frac{1 + \sin(\varphi_\beta)}{1 - \sin(\varphi_\beta)} \cdot \sigma_3, \beta \in [0, 90]; \sigma_3 \in [0, +\infty) \quad (11)$$

where $\sigma_{1cf\beta}$ is the peak strength with the bedding angle of β at various confining pressures.

To further verify the applicability and reliability of the M-C strength criteria, the theoretical peak strength under various confining pressures and different bedding angles was calculated according to Equation (11) (see Table 5).

Table 5. Calculation results of the M-C strength criteria under CTLT and TLUT.

Specimens No.	σ_3/MPa	β/°	Actual σ_{1cf}/MPa	Theoretical σ_{1cf}'/MPa	$\triangle\sigma_{1cf}$/MPa	$\triangle\chi$/%
UCT-0-0	0	0	70.5882	92.43275	21.84455	30.94646
UCT-0-30	0	30	63.1373	80.165336	17.02804	26.96985
UCT-0-45	0	45	36.4706	23.440632	13.02997	35.72732
UCT-0-60	0	60	52.1569	54.964666	2.807766	5.383307
UCT-0-90	0	90	75.2941	81.664869	6.370769	8.46118
CTLT-5-0	5	0	134.1575	117.3223	16.8352	12.54883
CTLT-5-30	5	30	128.512	105.304668	23.20733	18.05849
CTLT-5-45	5	45	95.6064	85.9217	9.6847	10.12976
CTLT-5-60	5	60	95.8986	82.16242	13.73618	14.32365
CTLT-5-90	5	90	108.722	104.13657	4.58543	4.217573
CTLT-10-0	10	0	164.289	142.21186	22.07714	13.43799
CTLT-10-30	10	30	155.263	130.443999	24.819	15.98514
CTLT-10-45	10	45	115.7094	109.82013	5.88927	5.089707
CTLT-10-60	10	60	120.081	109.36017	10.72083	8.927999
CTLT-10-90	10	90	135.1286	126.380968	8.747632	6.473561
CTLT-20-0	20	0	180.0923	191.990956	11.89866	6.606977
CTLT-20-30	20	30	174.4253	180.641627	6.216327	3.563891
CTLT-20-45	20	45	142.108	157.616989	15.50899	10.91352
CTLT-20-60	20	60	167.236	163.755675	3.480325	2.081086
CTLT-20-90	20	90	168.774	171.551677	2.777677	1.645797
TLUT-5-0	5	0	120.494	122.1011949	1.607195	1.333838
TLUT-5-30	5	30	110.902	95.9125784	14.98942	13.51592
TLUT-5-45	5	45	56.6327	86.7164127	30.08371	53.12075
TLUT-5-60	5	60	70.3082	64.87972	5.42848	7.720977
TLUT-5-90	5	90	76.7481	90.0899997	13.3419	17.38401
TLUT-10-0	10	0	132.48	131.547778	0.932222	0.70367
TLUT-10-30	10	30	131.083	115.597043	15.48596	11.81386
TLUT-10-45	10	45	88.451	114.902517	26.45152	29.90528
TLUT-10-60	10	60	125.119	90.267581	34.85142	27.85462
TLUT-10-90	10	90	136.373	117.256881	19.11612	14.01752
TLUT-20-0	20	0	149.447	150.390459	0.943459	0.6313
TLUT-20-30	20	30	170.939	154.96597	15.97303	9.344287
TLUT-20-45	20	45	143.667	114.902517	28.76448	20.02164
TLUT-20-60	20	60	153.784	141.026828	12.75717	8.295513
TLUT-20-90	20	90	166.376	171.590648	5.214648	3.134255

Among them, $\triangle\sigma_{1cf}$ represents the absolute strength difference between the theoretical peak strength σ_{1cf}' and the actual peak strength σ_{1cf}. Meanwhile, the percentage difference $\triangle\chi$ represents the ratio between the absolute difference of peak strength and the actual peak strength. Their specific expressions are as follows:

$$\Delta\sigma_{1cf} = \left|\sigma_{1cf}' - \sigma_{1cf}\right| \tag{12}$$

$$\Delta\chi = \frac{\left|\sigma_{1cf}' - \sigma_{1cf}\right|}{\sigma_{1cf}} \tag{13}$$

As shown in Table 5, in stress path CTLT, when the confining pressures were 0 MPa, 5 MPa, 10 MPa and 20 MPa, the averages of $\triangle\sigma_{1cf}$ were 12.081 MPa, 13.61 MPa, 14.45 MPa and 7.98 MPa, respectively, and the averages of $\triangle\chi$ were 21.498%, 11.86%, 9.98% and

4.96%, respectively. Correspondingly, in stress path CTLT, when the confining pressures were 5 MPa, 10 MPa and 20 MPa, the averages of $\triangle\sigma_{1cf}$ were 13.09 MPa, 19.37 MPa and 12.73 MPa, respectively, and the averages of $\triangle\chi$ were 18.62%, 16.86% and 8.29%, respectively. Additionally, the comparison between the theoretical curve and the actual test data of the M-C strength criteria is shown in Figures 10 and 11. According to the above comparative analysis, the evolution trend of the theoretical curve of M-C strength criteria was basically consistent with the actual test data. It indicated that the M-C strength criteria considering the bedding effect could be used to estimate the peak strength with different bedding angles.

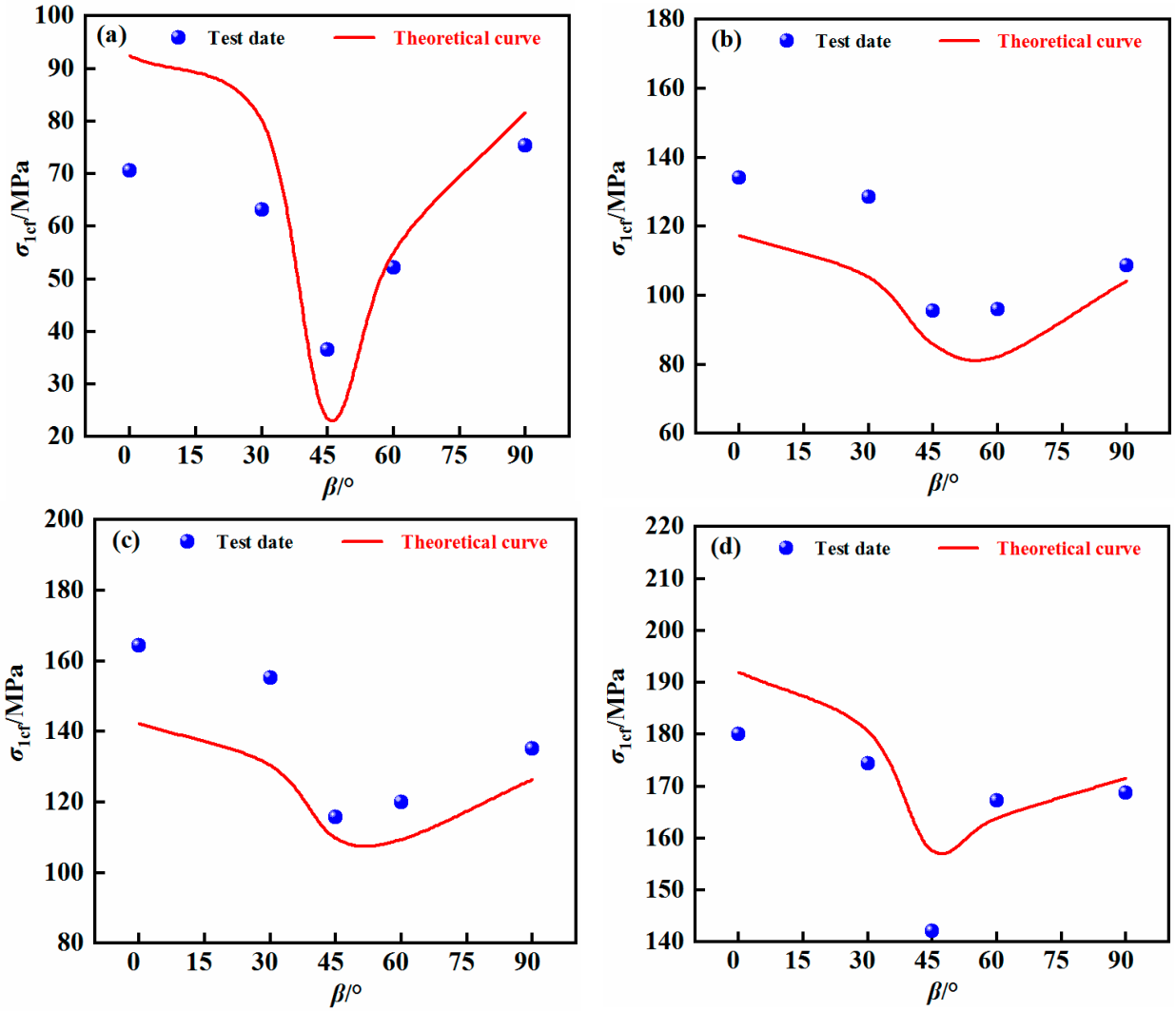

Figure 10. Comparison of the M-C strength criteria for theoretical curve and test data under UCT and CTLT: (**a**) σ_3 = 0 MPa; (**b**) σ_3 = 5 MPa; (**c**) σ_3 = 10 MPa; (**d**) σ_3 = 20 MPa.

3.3. Modified H-B Strength Criteria

The evolution trend of the M-C strength criteria considering anisotropy was basically consistent with the actual test values with the bedding angle, but there was still a great difference between the theoretical curve and the actual test values. Therefore, the H-B strength criteria were further considered and explored.

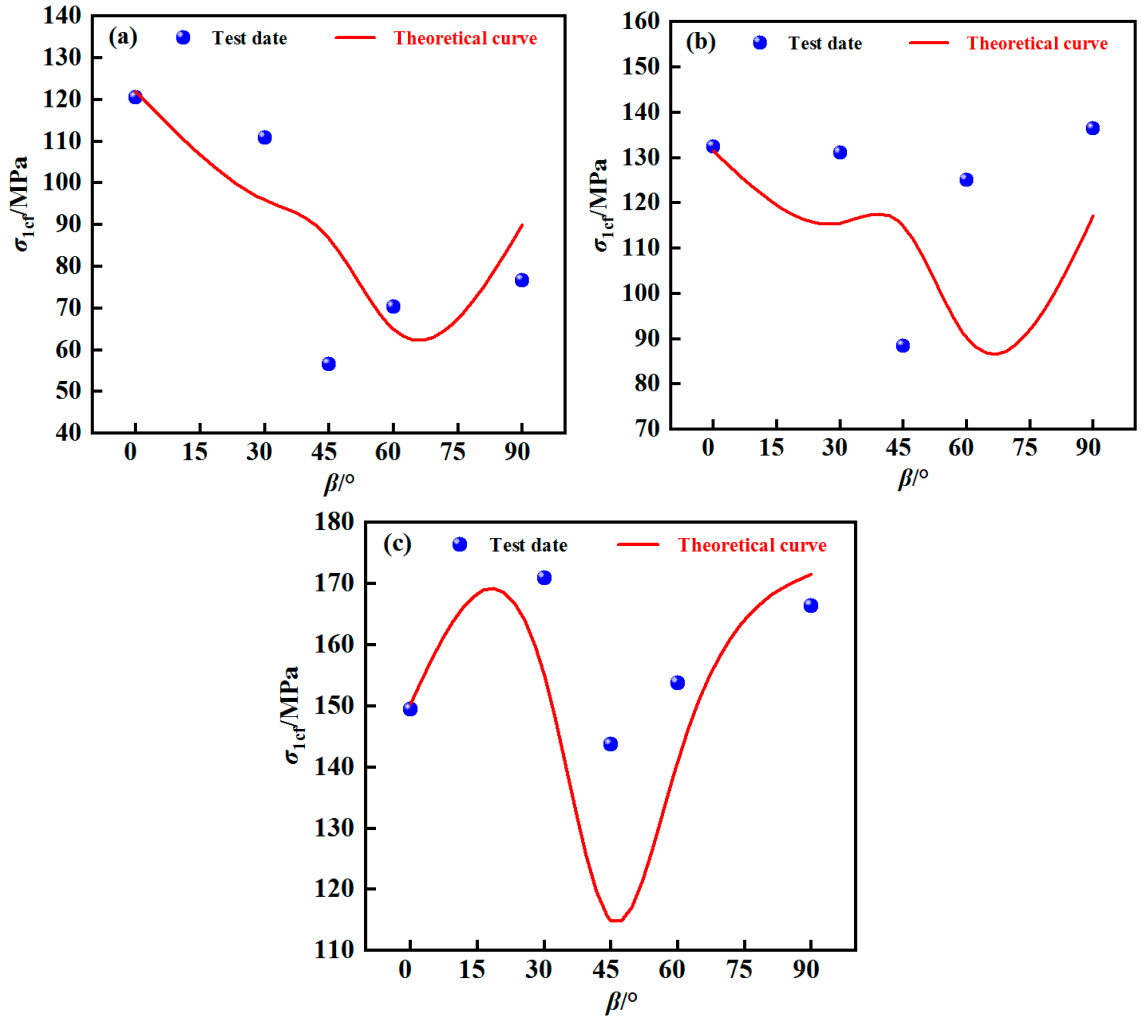

Figure 11. Comparison of the M-C strength criteria for theoretical curve and test data under TLUT: (**a**) σ_3 = 5 MPa; (**b**) σ_3 = 10 MPa; (**c**) σ_3 = 20 MPa.

3.3.1. Initial Principles of H-B Criteria

The H-B strength criteria were first proposed by Hoek and Brown in 1980 [48], and the specific expression is as follows [49,50]:

$$\sigma_{1cf} = \sigma_3 + \sigma_{UCS} \cdot \left(m \cdot \frac{\sigma_3}{\sigma_{UCS}} + n\right)^{\gamma} \tag{14}$$

where σ_{UCS}, σ_1 and σ_3 represent the uniaxial compressive strength, the peak strength and the confining pressure, respectively. For intact rocks, m is a constant, which can be used to reflect the level of rock hardness; n and γ are constants accompanying the rock mass to characterize its own properties. Especially, when the rock mass is intact, n = 1 and γ = 0.5. Therefore, for intact rocks, the specific expression of H-B strength criteria is as follows:

$$\sigma_{1cf} = \sigma_3 + \sigma_{UCS} \cdot \left(m \cdot \frac{\sigma_3}{\sigma_{UCS}} + 1\right)^{0.5} \tag{15}$$

3.3.2. Modified H-B Strength Criteria

To comprehensively consider the confining pressure effect and anisotropy on the peak strength under CTLT and TLUT, this study deeply explored the modified H-B strength criteria.

As shown in Figure 12, from the perspective of H-B strength criteria, the relationship between the deviatoric peak strength and the confining pressure was obtained. By comparing Equation (14), the fitting functions in Figure 12 and the attribute parameter (n), (γ) under CTLT and TLUT could be obtained. Additionally, due to all test specimens being layered sandstones, they could not be completely fitted according to Equation (15). Therefore, the fitting function relationship shown in Figure 12 needed to be modified by referring to the H-B strength criteria, and the corresponding specific details can be seen in Table 6, where A is the modified coefficient, and m is directly degraded to the uniaxial compressive strength with various bedding angles.

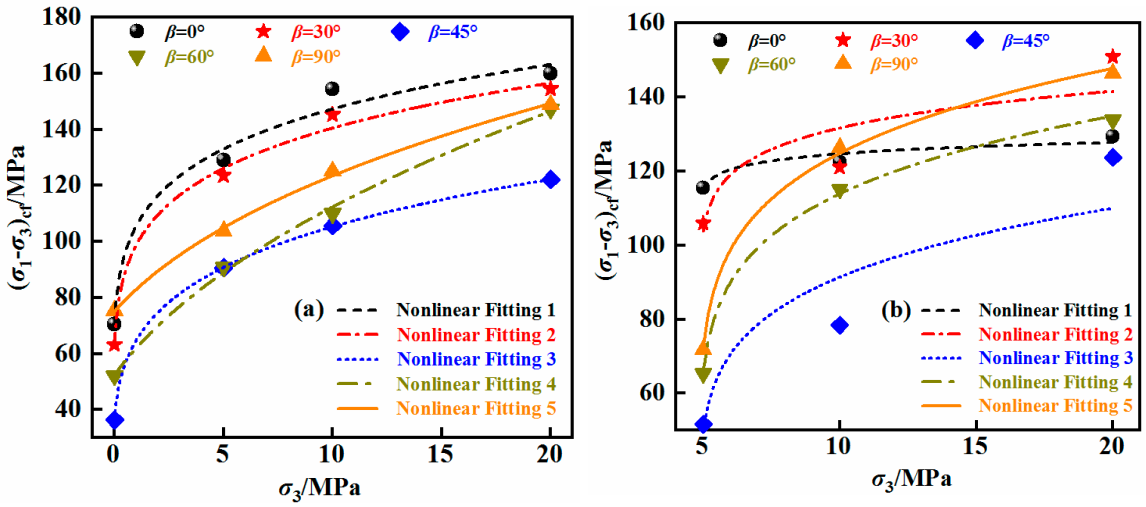

Figure 12. Fitting curves of deviator strength with various bedding angles in view of H-B strength criterion: (**a**) CTLT; (**b**) TLUT.

Therefore, according to the above analysis, the relationship between the peak strength of layered sandstones under CTLT and TLUT, the confining pressure and the bedding angle conformed to the modified H-B strength criteria, and the specific functional relationship is as follows:

$$\sigma_{1cf\beta} = \sigma_3 + A{\cdot}\sigma_{UCS-\beta}{\cdot}(\sigma_3 + n_\beta)^{\gamma_\beta} \quad (16)$$

where $\sigma_{UCS-\beta}$ is the uniaxial compressive strength of layered sandstones with the bedding angle of β.

Additionally, as shown in Figure 13, it was found that there was a certain functional relationship between the attribute parameters (n_β), (γ_β) and bedding angle; the specific expressions are as follows:

Table 6. Fitting functions between confining pressure and deviator strength of layered sandstones with different bedding angles under CTLT and TLUT.

Stress Path	β/°	Fitting Functions	R^2	A	n	γ
CTLT	0	$(\sigma_1-\sigma_3)_{cf}=1.482\sigma_{UCS-0}\times(\sigma_3+0.07026)^{0.14827}$	0.98537	1.482	0.07026	0.14827
	30	$(\sigma_1-\sigma_3)_{cf}=1.55\sigma_{UCS-30}\times(\sigma_3+0.06033)^{0.15641}$	0.99324	1.55	0.06033	0.15641
	45	$(\sigma_1-\sigma_3)_{cf}=1.753\sigma_{UCS-45}\times(\sigma_3+0.07447)^{0.21615}$	0.99995	1.753	0.07447	0.21615
	60	$(\sigma_1-\sigma_3)_{cf}=0.715\sigma_{UCS-60}\times(\sigma_3+2.16486)^{0.44159}$	0.99793	0.715	2.16486	0.44159
	90	$(\sigma_1-\sigma_3)_{cf}=0.71\sigma_{UCS-90}\times(\sigma_3+2.8149)^{0.32838}$	0.99846	0.71	2.8149	0.32838
TLUT	0	$(\sigma_1-\sigma_3)_{cf}=1.70\sigma_{UCS-0}\times(\sigma_3-4.85)^{0.0227}$	0.91955	1.70	−4.85	0.0227
	30	$(\sigma_1-\sigma_3)_{cf}=1.868\sigma_{UCS-30}\times(\sigma_3-4.85)^{0.06712}$	0.80546	1.868	−4.85	0.06712
	45	$(\sigma_1-\sigma_3)_{cf}=1.892\sigma_{UCS-45}\times(\sigma_3-4.85)^{0.17162}$	0.865	1.892	−4.85	0.17162

Table 6. *Cont.*

Stress Path	β/°	Fitting Functions	R^2	A	n	γ
TLUT	60	$(\sigma_1-\sigma_3)_{cf}=1.69\sigma_{UCS-60}\times(\sigma_3-4.85)^{0.15661}$	0.99893	1.69	−4.85	0.15661
	90	$(\sigma_1-\sigma_3)_{cf}=1.285\sigma_{UCS-90}\times(\sigma_3-4.85)^{0.15588}$	0.9986	1.285	−4.85	0.15588

Under CTLT and TLUT, for the parameter (γ_β):

$$\gamma_\beta = K + L\cdot\beta + O\cdot\beta^2 + U\cdot\beta^3 \tag{17}$$

Under CTLT, for the parameter (n_β):

$$n_\beta = G + H\cdot\beta + I\cdot\beta^2 + J\cdot\beta^3 \tag{18}$$

Under TLUT, for the parameter (n_β):

$$n_\beta = -4.85 \tag{19}$$

where K, L, O, U, G, H, I and J are fitting coefficients, and the corresponding coefficients are shown in Figure 13.

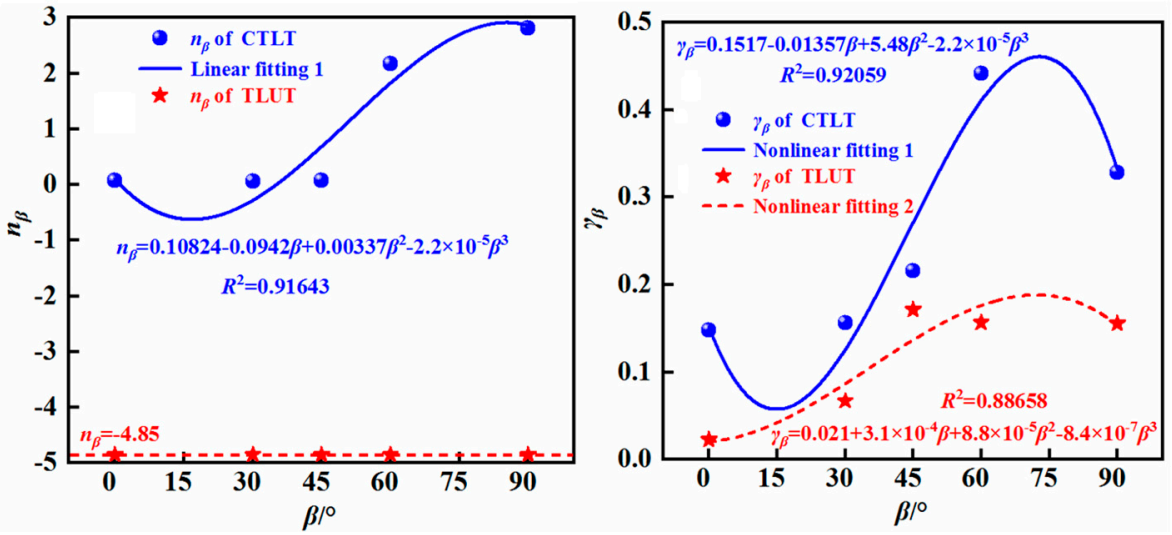

Figure 13. Variation of parameters n_β and γ_β of layered sandstones with various bedding angles β under CTLT and TLUT in view of modified H-B strength criteria.

Coupling Equations (16)–(18), the modified H-B strength criteria under CTLT could be obtained, and the specific expression was as follows:

$$\sigma_{1cf\beta} = \sigma_3 + A\cdot\sigma_{UCS-\beta}\cdot(\sigma_3+n_\beta)^{\gamma_\beta}\ \beta\in[0,90];\sigma_3\in[0,+\infty) \tag{20}$$

Coupling Equations (16), (17) and (19), the modified H-B strength criteria under TLUT could be obtained, and the specific expression was as follows:

$$\sigma_{1cf\beta} = \sigma_3 + A\cdot\sigma_{UCS-\beta}\cdot(\sigma_3-4.85)^{\gamma_\beta}\ \beta\in[0,90];\sigma_3\in[0,+\infty) \tag{21}$$

According to Equations (20) and (21), the theoretical peak strength under CTLT and TLUT could be calculated (see Table 7).

Table 7. Calculation results of the modified H-B strength criteria under CTLT and TLUT.

Specimens No.	σ_3/MPa	β/°	Actual σ_{1cf}/MPa	Theoretical σ_{1cf}'/MPa	$\triangle\sigma_{1cf}$/MPa	$\triangle\chi$/%
UCT-0-0	0	0	70.5882	70.56187	0.02633	0.037301
UCT-0-30	0	30	63.1373	63.12045	0.01685	0.026688
UCT-0-45	0	45	36.4706	36.468495	0.002105	0.005772
UCT-0-60	0	60	52.1569	52.450756	0.293856	0.563408
UCT-0-90	0	90	75.2941	75.096037	0.198063	0.263052
CTLT-5-0	5	0	134.1575	138.077143	3.919643	2.921673
CTLT-5-30	5	30	128.512	131.196554	2.684554	2.088952
CTLT-5-45	5	45	95.6064	95.825809	0.219409	0.229492
CTLT-5-60	5	60	95.8986	93.977556	1.921044	2.003203
CTLT-5-90	5	90	108.722	110.012396	1.290396	1.186877
CTLT-10-0	10	0	164.289	157.329419	6.959581	4.236182
CTLT-10-30	10	30	155.263	150.515898	4.747102	3.057459
CTLT-10-45	10	45	115.7094	115.338119	0.371281	0.320874
CTLT-10-60	10	60	120.081	122.409173	2.328173	1.938835
CTLT-10-90	10	90	135.1286	133.530415	1.598185	1.182714
CTLT-20-0	20	0	180.0923	183.191738	3.099438	1.721027
CTLT-20-30	20	30	174.4253	176.532883	2.107583	1.208301
CTLT-20-45	20	45	142.108	142.265970	0.15797	0.111162
CTLT-20-60	20	60	167.236	166.508056	0.727944	0.435279
CTLT-20-90	20	90	168.774	169.291193	0.517193	0.306441
TLUT-5-0	5	0	120.494	120.023404	0.470596	0.390556
TLUT-5-30	5	30	110.902	108.847201	2.054799	1.852806
TLUT-5-45	5	45	56.6327	54.820759	1.811941	3.199461
TLUT-5-60	5	60	70.3082	70.469598	0.161398	0.229558
TLUT-5-90	5	90	76.7481	76.950906	0.202806	0.264249
TLUT-10-0	10	0	132.48	134.636994	2.156994	1.628166
TLUT-10-30	10	30	131.083	141.665518	10.58252	8.073143
TLUT-10-45	10	45	88.451	101.4049927	12.95399	14.64539
TLUT-10-60	10	60	125.119	123.906407	1.212593	0.969152
TLUT-10-90	10	90	136.373	134.860098	1.512902	1.109385
TLUT-20-0	20	0	149.447	147.72747	1.71953	1.150595
TLUT-20-30	20	30	170.939	161.55488	9.38412	5.489748
TLUT-20-45	20	45	143.667	129.99982	13.66718	9.513096
TLUT-20-60	20	60	153.784	154.876549	1.092549	0.710444
TLUT-20-90	20	90	166.376	167.730403	1.354403	0.814062

As shown in Table 7, in stress path CTLT, when the confining pressures were 0 MPa, 5 MPa, 10 MPa and 20 MPa, the averages of $\triangle\sigma_{1cf}$ were 0.10744 MPa, 2.007 MPa, 3.20 MPa and 1.322 MPa, respectively, and the averages of $\triangle\chi$ were 0.179%, 1.686%, 2.147% and 0.756%, respectively. Correspondingly, in stress path TLUT, when the confining pressures were 5 MPa, 10 MPa and 20 MPa, the averages of $\triangle\sigma_{1cf}$ were 0.94 MPa, 5.683 MPa and 5.44 MPa, respectively, and the averages of $\triangle\chi$ were 1.187%, 5.285% and 3.536%, respectively. Additionally, the comparison between the theoretical curve and the actual test data of the modified H-B strength criteria under CTLT and TLUT is shown in Figures 14 and 15. According to the above comparative analysis, the evolution trend of the theoretical curve of modified H-B strength criteria was basically consistent with the actual test data. Furthermore, compared with the M-C strength criteria, the accuracy and reliability of the modified H-B strength criteria were significantly higher. It indicated that the modified H-B strength criteria were more appropriate to estimate the peak strength of layered sandstones.

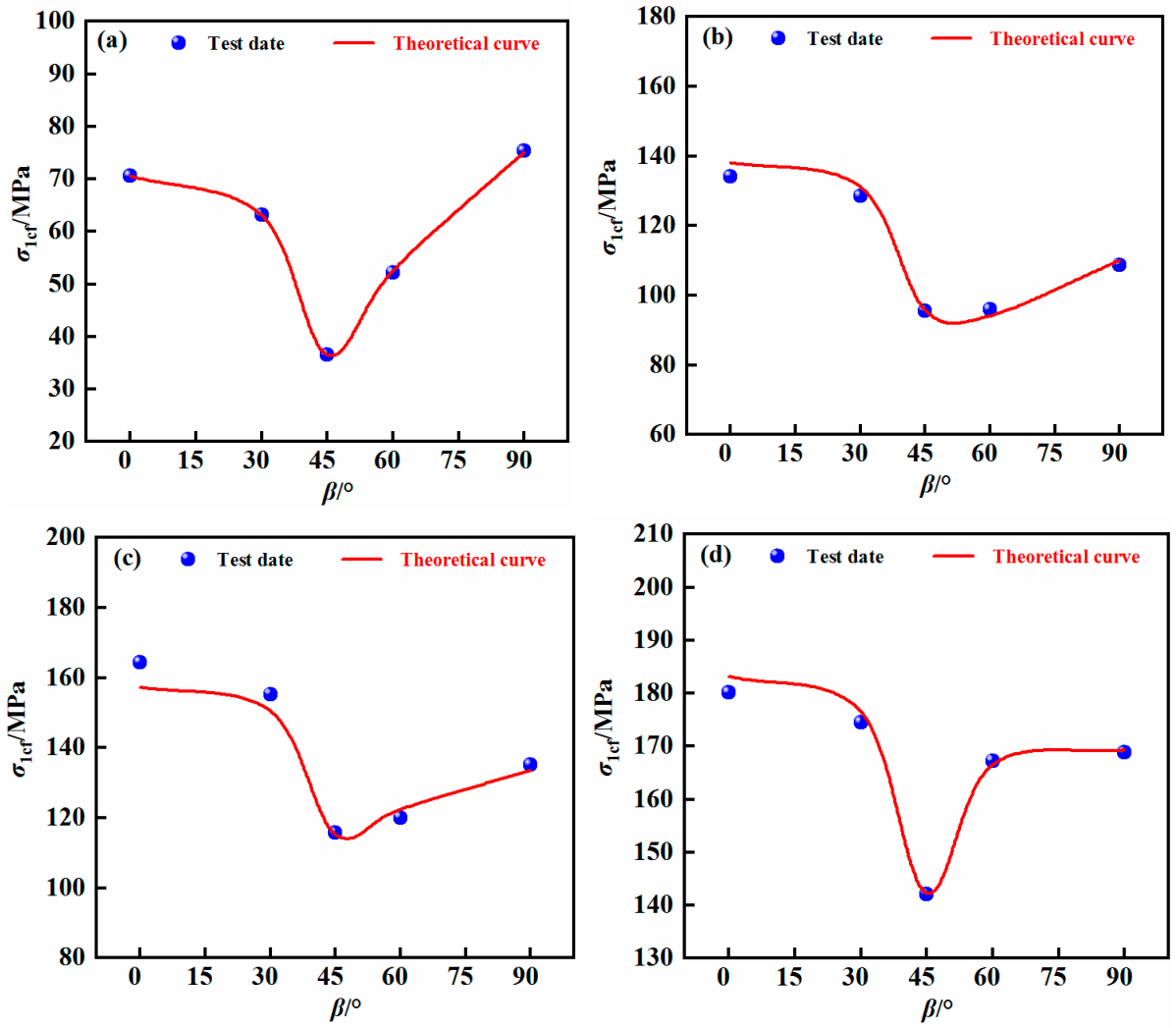

Figure 14. Comparison of the modified H-B strength criteria for theoretical curve and test data under UCT and CTLT: (**a**) σ_3 = 0 MPa; (**b**) σ_3 = 5 MPa; (**c**) σ_3 = 10 MPa; (**d**) σ_3 = 20 MPa.

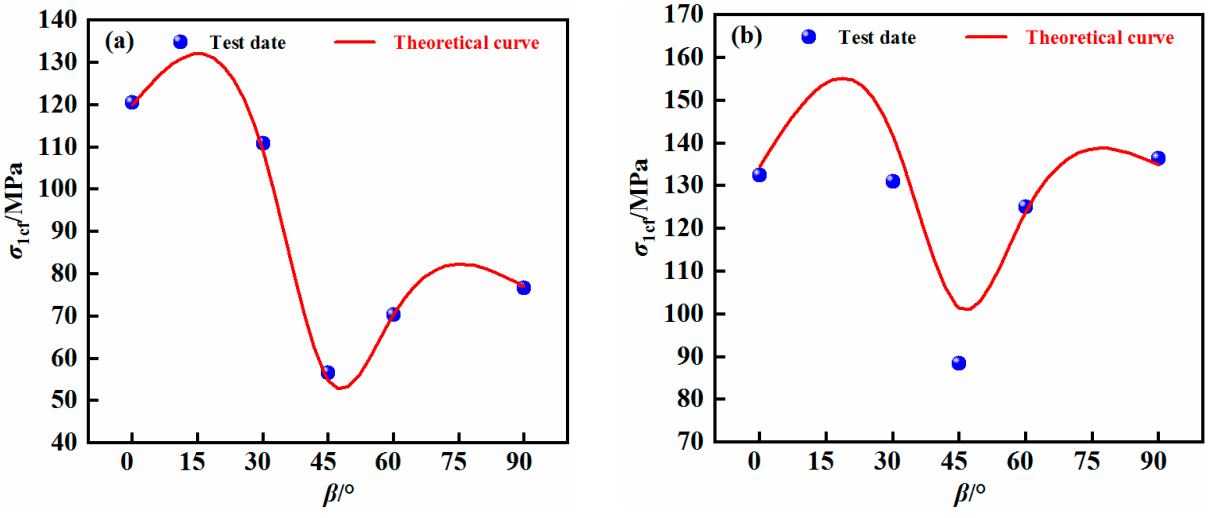

Figure 15. *Cont.*

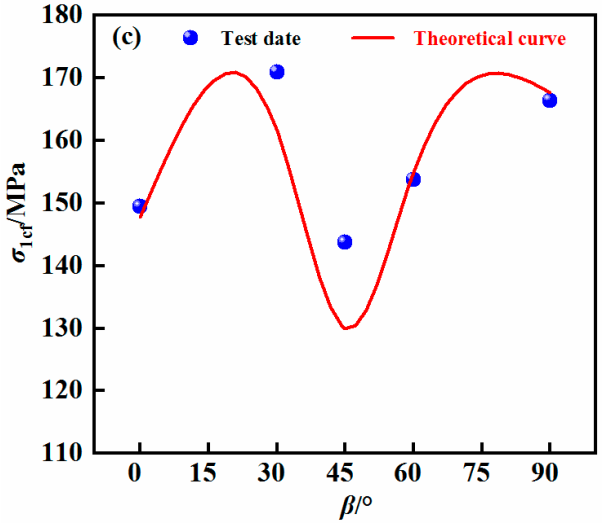

Figure 15. Comparison of the modified H-B strength criteria for theoretical curve and test data under TLUT: (**a**) σ_3 = 5 MPa; (**b**) σ_3 = 10 MPa; (**c**) σ_3 = 20 MPa.

4. Discussion

The M-C and the modified H-B strength criteria were established. Due to the limitations in the types of rocks and the quantity of test data, the criteria obtained herein are only preliminary. Therefore, two aspects regarding the research need to be further emphasized.

First, for intact rocks, the parameters (n) and (γ) in the H-B strength criteria are 1 and 0.5, respectively, which are constants [51–55]. Nevertheless, layered sandstone was used in this study which suffered from high initial stress state and had significant anisotropy, leading to the modification of H-B strength criteria. Among them, the parameters (n) and (γ) in the modified H-B strength criteria had a strong nonlinear function relationship with the bedding angle. It indicated that the anisotropy could significantly affect the accuracy and reliability of rock strength criteria. Meanwhile, the geological situation in actual engineering is extremely complicated, and complex structures with weak planes such as joints, cleats and bedding are all over the sites. Therefore, it was necessary to deeply conduct the identification and characterization of the rock samples (especially those containing bedding, cleats, joints and other series of similar structures) before conducting numerous mechanical tests. In this way, it could not only avoid blindly identifying the integrity of test samples, but also provide reliable criterion for accurate analysis of rock strength criteria and the rock failure mechanism in the later stage.

Additionally, the unloading effect could significantly affect the cohesion, internal friction angle and the peak strength. Nevertheless, it was easy to ignore the influences of the unloading effect on the rock strength criteria [56–61]. Therefore, a study perspective considering the unloading effect of rocks should be deeply considered to establish the rock strength criteria in the later stage. In this way, it is expected that further breakthroughs and improvement in the accuracy and reliability of field engineering applications will be achieved.

5. Conclusions

(1) With increasing bedding angle, the peak strength first decreased and then increased. When the bedding angle was 45°, the peak strength was the smallest. In addition, with increasing confining pressure, the peak strength also showed a continuous increasing nonlinear evolution trend. Additionally, the peak strength under TLUT was significantly lower than that under CTLT;

(2) With increasing bedding angle, the cohesion with CTLT decreased first and then increased, while the evolution trend of the internal friction angle with CTLT was opposite. Additionally, with increasing bedding angle, the cohesion with TLUT also

decreased first and then increased, but the cohesion with TLUT increased first, then decreased, and finally increased again;

(3) The cohesion and internal friction angle, parameters (n) and (γ), were not constants and changed with increasing bedding angle. Compared with CTLT, the variation degree of the cohesion and internal friction angle under TLUT was more significant with increasing bedding angle;

(4) Compared with the M-C strength criteria, the modified H-B strength criteria were more suitable to estimate the peak strength of layered sandstones.

Author Contributions: Z.S.: Conceptualization, Investigation, Methodology, Software, Data curation, Writing—original draft and Writing—review and editing. J.Z.: Writing—review and editing, Funding acquisition, Visualization, Supervision. S.W.: Visualization, Investigation. All authors have read and agreed to the published version of the manuscript.

Funding: This study was supported by the National Natural Science Foundation of China (grant nos. 52034009, 51974319), the Yue Qi Distinguished Scholar Project (grant no. 2020JCB01), the National Key R & D Program of China (grant no. 2022YFC3004602) and China University of Mining and Technology (Beijing) Fundamental Research Fund—Top Innovative Talents Cultivation Fund for Doctoral Students (grant no. BBJ2023001).

Institutional Review Board Statement: Not applicable.

Informed Consent Statement: Not applicable.

Data Availability Statement: Not applicable.

Conflicts of Interest: The authors declare no conflict of interest.

References

1. Genis, M.; Basarir, H.; Ozarslan, A.; Bilir, E.; Balaban, E. Engineering geological appraisal of the rock masses and preliminary support design, Dorukhan Tunnel, Zonguldak, Turkey. *Eng. Geol.* **2007**, *92*, 14–26. [CrossRef]
2. Xue, Y.G.; Zhang, X.L.; Li, S.C.; Qiu, D.H.; Su, M.X.; Li, L.P.; Li, Z.Q.; Tao, Y.F. Analysis of factors influencing tunnel deformation in loess deposits by data mining: A deformation prediction model. *Eng. Geol.* **2018**, *232*, 94–103. [CrossRef]
3. Feng, S.J.; Zhao, Y.; Zhang, X.L.; Bai, Z.B. Leachate leakage investigation, assessment and engineering countermeasures for tunneling underneath a MSW landfill. *Eng. Geol.* **2020**, *265*, 105447. [CrossRef]
4. Liu, D.Q.; Ling, K.; Guo, C.B.; He, P.F.; He, M.C.; Sun, J.; Yan, X.H. Experimental simulation study of rockburst characteristics of Sichuan-Tibet granite: A case study of the Zheduoshan tunnel. *Eng. Geol.* **2022**, *305*, 106701. [CrossRef]
5. Tao, J.; Yang, X.G.; Ding, P.P.; Li, X.L.; Zhou, J.W.; Lu, G.D. A fully coupled thermo-hydro-mechanical-chemical model for cemented backfill application in geothermal conditions. *Eng. Geol.* **2022**, *302*, 106643. [CrossRef]
6. Benavente, D.; Garcia, D.; Cura, M.A.; Fort, R.; Ordonez, S. Durability estimation of porous building stones from pore structure and strength. *Eng. Geol.* **2004**, *74*, 113–127. [CrossRef]
7. Hecht, C.A.; Bonsch, C.; Bauch, E. Relations of rock structure and composition to petrophysical and geomechanical rock properties: Examples from permocarboniferou red-beds. *Rock. Mech. Rock. Eng.* **2005**, *38*, 197–216. [CrossRef]
8. Sabatakakis, N.; Koukis, G.; Tsiambaos, G.; Papanakli, S. Index properties and strength variation controlled by microstructure for sedimentary rocks. *Eng. Geol.* **2008**, *97*, 80–90. [CrossRef]
9. Torok, A.; Vasarhelyi, B. The influence of fabric and water content on selected rock mechanical parameters of travertine, examples from Hungary. *Eng. Geol.* **2010**, *115*, 237–245. [CrossRef]
10. Shen, J.Y.; Jimenez, R.; Karakus, M.; Xu, C.S. A simplified failure criterion for intact rocks based on rock type and uniaxial compressive strength. *Rock. Mech. Rock. Eng.* **2014**, *47*, 357–369. [CrossRef]
11. Shen, J.Y.; Karakus, M. Simplified method for estimating the Hoek-Brown constant for intact rocks. *J. Geotech. Geoenviron.* **2014**, *140*, 971–984. [CrossRef]
12. Rajabzadeh, M.A.; Moosavinasab, Z.; Rakhshandehroo, G. Effects of rock classes and porosity on the relation between uniaxial compressive strength and some rock properties for Carbonate rocks. *Rock. Mech. Rock. Eng.* **2012**, *45*, 113–122. [CrossRef]
13. Wang, Y.F.; Cui, F. Energy evolution mechanism in process of sandstone failure and energy strength criterion. *J. Appl. Geophys.* **2018**, *154*, 21–28. [CrossRef]
14. Li, Z.; Zhou, H.; Hu, D.W.; Zhang, C.Q. Yield criterion for rocklike geomaterials based on strain energy and CMP model. *Int. J. Geomech.* **2020**, *20*, 04020013. [CrossRef]
15. Sari, M. An improved method of fitting experimental data to the Hoek–Brown failure criterion. *Eng. Geol.* **2012**, *127*, 27–35. [CrossRef]

16. Fjaer, E.; Ruistuen, H. Impact of the intermediate principal stress on the strength of heterogeneous rock. *J. Geophys. Res.* **2002**, *107*, 2032. [CrossRef]
17. Priest, S.D. Determination of shear strength and three-dimensional yield strength for the Hoek-Brown criterion. *Rock. Mech. Rock. Eng.* **2005**, *38*, 299–327. [CrossRef]
18. Zhang, Q.; Zhu, H.H. Collaborative 3D geological modeling analysis based on multi-source data standard. *Eng. Geol.* **2018**, *246*, 233–244. [CrossRef]
19. Saroglou, H.; Tsiambaos, G. A modified Hoek-Brown failure criterion for anisotropic intact rock. *Int. J. Rock. Mech. Min. Sci.* **2008**, *45*, 223–234. [CrossRef]
20. Singh, M.; Raj, A.; Singh, B. Modified Mohr-Coulomb criterion for non-linear triaxial and poly-axial strength of intact rocks. *Int. J. Rock. Mech. Min. Sci.* **2011**, *48*, 546–555. [CrossRef]
21. Zhou, C.T.; Xu, C.S.; Karakus, M.; Shen, J.Y. A particle mechanics approach for the dynamic strength model of the jointed rock mass considering the joint orientation. *Int. J. Numer. Anal. Met.* **2019**, *43*, 2797–2815. [CrossRef]
22. Zhou, C.T.; Xie, H.P.; Zhu, J.B.; Zhou, T. Failure criterion considering high temperature treatment for rocks from a micromechanical perspective. *Theor. Appl. Fract. Mec.* **2022**, *118*, 103226. [CrossRef]
23. Wang, G.S.; Lu, D.C.; Du, X.L.; Zhao, X. Dynamic multiaxial strength criterion for concrete based on strain rate–dependent strength parameters. *J. Eng. Mech.* **2018**, *144*, 04018018. [CrossRef]
24. Wang, G.S.; Lu, D.C.; Li, M.; Zhao, X.; Wang, J.T.; Du, X.L. Static–dynamic combined multiaxial strength criterion for concrete. *J. Eng. Mech.* **2021**, *147*, 04021017. [CrossRef]
25. Yang, Q.; Zan, Y.W.; Xie, L.G. Comparative analysis of the nonlinear unified strength criterion for rocks and other three-dimensional Hoek-Brown strength criteria. *Geomech. Geophysics. Geo.* **2018**, *4*, 29–37. [CrossRef]
26. Zhang, Q.; Li, C.; Jiang, B.S. New true-triaxial rock strength criteria considering intrinsic material characteristics. *Acta Mech. Sinica.* **2018**, *34*, 138–150. [CrossRef]
27. Song, Z.L.; Li, M.H.; Yin, G.Z.; Ranjith, P.G.; Liu, C. Rock strength criterion considering the effect of hydrostatic stress on lode angle effect. *Energy. Sci. Eng.* **2019**, *7*, 1166–1177. [CrossRef]
28. Song, Z.L.; Yin, G.Z.; Ranjith, P.G.; Li, M.H.; Huang, J.; Liu, C. Influence of the intermediate principal stress on sandstone failure. *Rock. Mech. Rock. Eng.* **2019**, *52*, 3033–3046. [CrossRef]
29. Zhang, Q.G.; Yao, B.W.; Fan, X.Y.; Li, Y.; Li, M.H.; Zeng, F.T.; Zhao, P.F. A modified Hoek-Brown failure criterion for unsaturated intact shale considering the effects of anisotropy and hydration. *Eng. Fract. Mech.* **2020**, *241*, 107369. [CrossRef]
30. Lee, Y.K.; Bobet, A. Instantaneous friction angle and cohesion of 2-D and 3-D Hoek-Brown rock failure criteria in terms of stress invariants. *Rock. Mech. Rock. Eng.* **2014**, *47*, 371–385. [CrossRef]
31. Yin, Q.; Liu, R.C.; Jing, H.W.; Su, H.J.; Yu, L.Y.; He, L.X. Experimental study of nonlinear flow behaviors through fractured rock samples after high-temperature exposure. *Rock. Mech. Rock. Eng.* **2019**, *52*, 2963–2983. [CrossRef]
32. Yin, Q.; Wu, J.Y.; Zhu, C.; He, M.C.; Meng, Q.X.; Jing, H.W. Shear mechanical responses of sandstone exposed to high temperature under constant normal stiffness boundary conditions. *Geomech. Geophysics. Geo.* **2021**, *7*, 1–17. [CrossRef]
33. Yin, Q.; Wu, J.Y.; Zhu, C.; Wang, Q.; Xie, J.Y. The role of multiple heating and water cooling cycles on physical and mechanical responses of granite rocks. *Geomech. Geophysics. Geo.* **2021**, *7*, 69. [CrossRef]
34. Pan, J.L.; Zhang, Y.; Li, P.; Wu, X.; Xi, X. Mechanical properties and thermo-chemical damage constitutive model of granite subjected to thermal and chemical treatments under uniaxial compression. *Constr. Build. Mater.* **2023**, *390*, 131755. [CrossRef]
35. Pan, J.L.; Cai, M.F.; Li, P.; Guo, Q.F. A damage constitutive model of rock-like materials containing a single crack under the action of chemical corrosion and uniaxial compression. *J. Cent. South. Univ.* **2022**, *29*, 486–498. [CrossRef]
36. Zhang, J.W.; Song, Z.X.; Wang, S.Y. Mechanical behavior of deep sandstone under high stress-seepage coupling. *J. Cent. South. U.* **2021**, *28*, 3190–3206. [CrossRef]
37. Song, Z.X.; Zhang, J.W.; Zhang, L.C.; Dong, X.K.; Niu, W.M.; Zhang, Y. The permeability properties of bedded coal and rock: Review and new insights. *Energy. Sci. Eng.* **2022**, *10*, 1544–1565. [CrossRef]
38. Song, Z.X.; Zhang, J.W.; Wang, S.Y.; Dong, X.K.; Zhang, Y. Energy evolution characteristics and weak structure—"Energy Flow" impact damaged mechanism of deep-bedded sandstone. *Rock Mech. Rock Eng.* **2023**, *56*, 2017–2047. [CrossRef]
39. Song, Z.X.; Zhang, J.W.; Zhang, Y.; Dong, X.K.; Wang, S.Y. Characterization and evaluation of brittleness of deep bedded sandstone from the perspective of the whole life-cycle evolution process. *Int. J. Min. Sci. Technol.* **2023**, *33*, 481–502. [CrossRef]
40. Erener, A.; Mutlu, A.; Düzgün, H.S. A comparative study for landslide susceptibility mapping using GIS-based multi-criteria decision analysis (MCDA), logistic regression (LR) and association rule mining (ARM). *Eng. Geol.* **2016**, *203*, 45–55. [CrossRef]
41. Sepehri, M.; Apel, D.B.; Adeeb, S.; Leveille, P.; Hall, R.A. Evaluation of mining-induced energy and rockburst prediction at a diamond mine in Canada using a full 3D elastoplastic finite element model. *Eng. Geol.* **2020**, *266*, 105457. [CrossRef]
42. Kokkala, A.; Marinos, V. An engineering geological database for managing, planning and protecting intelligent cities: The case of Thessaloniki city in Northern Greece. *Eng. Geol.* **2022**, *301*, 106617. [CrossRef]
43. He, M.C. Physical modeling of an underground roadway excavation in geologically 45° inclined rock using infrared thermography. *Eng. Geol.* **2011**, *121*, 165–176. [CrossRef]
44. Torresa, F.; Piccinini, L.; Pola, M.; Zampieri, D.; Fabbri, P. 3D hydrogeological reconstruction of the fault-controlled Euganean Geothermal System (NE Italy). *Eng. Geol.* **2020**, *274*, 105740. [CrossRef]

45. Saeidi, O.; Vaneghi, R.G.; Rasouli, V.; Gholami, R. A modified empirical criterion for strength of transversely anisotropic rocks with metamorphic origin. *Bull. Eng. Geol. Environ.* **2013**, *72*, 257–269. [CrossRef]
46. Zhao, J. Applicability of Mohr–Coulomb and Hoek–Brown strength criteria to the dynamic strength of brittle rock. *Int. J. Rock. Mech. Min. Sci.* **2000**, *37*, 1115–1121. [CrossRef]
47. Liu, X.W.; Liu, Q.S.; Kang, Y.S.; Pan, Y.C. Improved nonlinear strength criterion for jointed rock masses subject to complex stress states. *Int. J. Geomech.* **2018**, *18*, 04017164. [CrossRef]
48. Hoek, E.; Brown, E.T. *Underground Excavation in Rock*; Institution of Mining and Metallurgy: London, UK, 1980.
49. Hoek, E.; Brown, E.T. Practical estimates of rock mass strength. *Int. J. Rock. Mech. Min. Sci.* **1997**, *34*, 1165–1186. [CrossRef]
50. Hoek, E.; Brown, E.T. The Hoek-Brown failure criterion and GSI-2018 edition. *J. Rock. Mech. Geotech. Eng.* **2018**, *37*, 1–28. [CrossRef]
51. Peng, J.; Cai, M.F. A cohesion loss model for determining residual strength of intact rocks. *Int. J. Rock. Mech. Min. Sci.* **2019**, *119*, 131–139. [CrossRef]
52. Alejano, L.A.; Walton, G.; Gaines, S. Residual strength of granitic rocks. *Tunn. Undergr. Sp. Tech.* **2021**, *118*, 104189. [CrossRef]
53. Shi, X.C.; Yang, X.; Meng, Y.F.; Li, G. Modified Hoek-Brown failure criterion for anisotropic rocks. *Environ. Earth. Sci.* **2016**, *75*, 995.1–995.11. [CrossRef]
54. He, M.M.; Zhang, Z.Q.; Zhu, J.W.; Li, N. Correlation between the constant mi of Hoek-Brown criterion and porosity of intact rock. *Rock. Mech. Rock. Eng.* **2022**, *55*, 923–936. [CrossRef]
55. Luo, B.Y.; Ye, Y.C.; Hu, N.Y.; Wang, W.Q. Investigation of dip effect on uniaxial compressive strength of inclined rock sample by experimental and theoretical models. *Rock. Mech. Rock. Eng.* **2020**, *53*, 1–17. [CrossRef]
56. Shen, B.T.; Shi, J.Y.; Barton, N. Graphic examples of a logical nonlinear strength criterion for intact rock. *Rock. Mech. Rock. Eng.* **2019**, *53*, 71–75. [CrossRef]
57. Singh, M.; Singh, B. Modified Mohr-Coulomb criterion for non-linear triaxial and poly-axial strength of jointed rocks. *Int. J. Rock. Mech. Min. Sci.* **2012**, *51*, 43–52. [CrossRef]
58. Barton, N. Shear strength criteria for rock, rock joints, rockfill and rock masses: Problems and some solutions. *J. Rock. Mech. Geotech. Eng.* **2013**, *5*, 249–261. [CrossRef]
59. Poulsen, B.A.; Adhikary, D.P.; Elmouttie, M.K.; Wilkins, A. Convergence of synthetic rock mass modelling and the Hoek-Brown strength criterion. *Int. J. Rock. Mech. Min. Sci.* **2015**, *80*, 171–180. [CrossRef]
60. Tsiambaos, G.; Saroglou, H. Excavatability assessment of rock masses using the geological strength index (GSI). *Bull. Eng. Geol. Environ.* **2010**, *69*, 13–27. [CrossRef]
61. Kang, H.P. Temporal scale analysis on coal mining and strata control technologies. *J. Min. Strata. Control. Eng.* **2021**, *3*, 5–27.